



**HAL**  
open science

# Time and frequency response of structures with frequency dependent, non-proportional linear damping

Lionel Zoghaib, Pierre-Olivier Mattei

► **To cite this version:**

Lionel Zoghaib, Pierre-Olivier Mattei. Time and frequency response of structures with frequency dependent, non-proportional linear damping. *Journal of Sound and Vibration*, 2014, 333 (3), pp.887-900. 10.1016/j.jsv.2013.09.044 . hal-01024496

**HAL Id: hal-01024496**

**<https://hal.science/hal-01024496>**

Submitted on 17 Jul 2014

**HAL** is a multi-disciplinary open access archive for the deposit and dissemination of scientific research documents, whether they are published or not. The documents may come from teaching and research institutions in France or abroad, or from public or private research centers.

L'archive ouverte pluridisciplinaire **HAL**, est destinée au dépôt et à la diffusion de documents scientifiques de niveau recherche, publiés ou non, émanant des établissements d'enseignement et de recherche français ou étrangers, des laboratoires publics ou privés.

1           Time and frequency response of structures with  
2 frequency dependent, non-proportional linear damping

3                           L. Zoghaib<sup>a</sup>, P.-O. Mattei<sup>b,\*</sup>

4   <sup>a</sup>*EADS, 12 rue Pasteur, 92150 Suresnes, France*

5   <sup>b</sup>*LMA, CNRS, UPR 7051, Aix-Marseille Univ, Centrale Marseille, F-13402 Marseille*  
6   *Cedex 20, France*

---

7   **Abstract**

A method to compute the non-stationary time and frequency response of structures with a frequency-dependent non-proportional linear damping, called the resonance modes method, is presented in this paper. It consists of two main steps. The first step aims at spotting the structure resonance modes, which are the solutions of the matrix non-linear eigenvalue problem obtained using the finite element method in the complex plane. This step requires a complex eigensolver and an iterative scheme, a perturbation technique or a combination of both. The second step uses the computed resonance modes and an analytical expression of the inverse Laplace transform to deduce the time or frequency response of structures to general excitations. The response of an aluminum plate damped with an elastomer treatment to a point-force excitation, computed with the classical modal approach, the direct solution and the presented method shows its precision and efficiency. An acoustic power computation finally validates the implementation of a fast variant, based on the perturbation technique, for vibroacoustic applications.

8   *Keywords:* Damping, elastomer, vibroacoustic, complex modes

---

---

\*Corresponding author

*Email addresses:* [lionel.zoghaib@eads.net](mailto:lionel.zoghaib@eads.net) (L. Zoghaib),  
[mattei@lma.cnrs-mrs.fr](mailto:mattei@lma.cnrs-mrs.fr) (P.-O. Mattei )

*Preprint submitted to Elsevier*

*July 17, 2014*

## 9 1. Introduction

10 The modeling of damped structures is still a very active research field.  
11 The main reason is that most numerical methods available today have a  
12 number of limitations. Time approaches are excessively costly compared  
13 to frequency approaches, while frequency approaches are often reduced  
14 to stationary excitation types or are restricted to specific damping mod-  
15 els. Some finite element codes can now take advantage of complex eigen-  
16 solvers, adapted to non-proportionally damped systems, but they do not  
17 offer any consistent approach to deduce the response to dynamic load-  
18 ings from the computed complex modes. A better handling of complex  
19 frequency-dependent eigenvalue problems, which stem from the viscoelastic  
20 constitutive equations written in the complex plane is however needed by  
21 the industry. In aeronautics, in particular, lighter damping treatments with  
22 enhanced efficiency need to be further developed. Five main types of meth-  
23 ods with different levels of approximation are currently available to address  
24 the problem of viscoelasticity in dynamics: direct solutions, methods based  
25 on modal strain energy, perturbation-based methods, state space methods  
26 and finally methods introducing dissipation coordinates.

27  
28 The direct solution is often the only option to model viscoelastic behavior  
29 in standard finite element codes with accuracy, but unfortunately at high  
30 numerical cost. A number of variants have been developed, though, which  
31 make the method become more practical over time. The Padé method, in-  
32 vestigated by Chazot *et al* [1] for instance, allows an efficient reconstruction  
33 of the frequency response function with a substantial speed up gain.

34  
35 Modal Strain Energy analysis (MSE), in its initial form, is based on the  
36 eigenvector basis of the undamped structure with no frequency dependence.  
37 It has been used by Finegan and Gibson [2], for instance, to characterize  
38 the damping loss factor of composite structures with coated fiber reinforce-  
39 ment; their approach takes the contribution of the fibers, fibers coating and

40 composite matrix damping separately to assess total damping. Using the  
41 MSE analysis, one needs to compute the modal strain energy of the different  
42 structure sub-systems in a first step; each energy is then weighted by the  
43 sub-system's loss factor. Summing all weighted energies and dividing the  
44 result by the total modal strain energy finally yields the structure's modal  
45 damping. MSE analysis requires the vectors of the undamped system to be  
46 very close to those of the damped system. Moreover, it is only valid when  
47 a uniform loss factor mean value can be associated with a sub-system. For  
48 this reason, non-local dissipations such as noise radiation energy loss can  
49 not be properly considered.

50

51 Damping non-proportionality is caused by inhomogeneous damping distri-  
52 butions. A complex eigensolver is needed in this case to compute the struc-  
53 ture's complex modes. Perturbation techniques, contrary to MSE analysis,  
54 can be used to handle non-proportionality, as pointed out by Woodhouse [3],  
55 or more recently by Cha [4] for arbitrarily damped nearly proportional sys-  
56 tems. If the damping is slightly non-proportional, indeed, an approximation  
57 of the complex eigenvectors can be deduced from the undamped structure  
58 modal basis. Another alternative for solving complex eigenvalue problems is  
59 to use the state space method (Hurty and Rubinstein [5]). The method takes  
60 non-proportionality into account with no limiting assumption. It therefore  
61 gives accurate complex eigensolutions using a real eigensolver only. The  
62 main drawback of the method, though, is the matrix size doubling that re-  
63 sults in prohibitive calculation times for large systems. The method does  
64 not handle frequency dependence either. Alternatively, Adhikari [6] pro-  
65 posed an approach that uses the undamped system normal modes obtained  
66 from a real eigensolver to deduce complex modes iteratively, and Cortés and  
67 Elejabarrieta [7] suggested an approximate method to compute them from  
68 the undamped solutions by finite increments using eigenvector derivatives  
69 and the Rayleigh quotient.

70

71 The last approach available currently uses analytical viscoelastic models to  
72 reshape any frequency-dependent complex problem into a real frequency-  
73 independent equivalent one. Dissipation coordinates that characterize an  
74 intermediate field need to be introduced. These coordinates are written ex-  
75 plicitly with respect to other coordinates and a given complex viscoelastic  
76 model. The GHM method (Golla Hughes Mac Tavish, Golla and Hughes  
77 [8], Barbosa and Farage [9]) or the ADF method (Anelastic Displacement  
78 Field, Lesieutre and Bianchini [10]) are different variants of this approach.  
79 They offer a number of advantages: damping can be frequency-dependent,  
80 non-proportional; numerically, only a standard real eigensolver is needed.  
81 The main drawback, however, is numerical: matrices become larger and un-  
82 symmetric; also, the use of specific damping models restricts the approach  
83 generality.

84

85 The resonance modes method presented here, like GHM and ADF meth-  
86 ods, not only handle frequency dependence and non-proportional damping  
87 but also remediates most of their disadvantages; damping, in particular,  
88 can remain general. It falls in the wide category of extended modal ap-  
89 proaches such as the modal contribution functions superposition method  
90 proposed by Cortés and Elejabarrieta [11], the modal approach combined  
91 with fractional derivatives in the paper by Sorrentino and Fasana [12], or  
92 the fast frequency response analysis algorithm suggested by Kim [13], valid  
93 in the case of partially damped structures. Introduced initially to handle  
94 radiation frequency dependence in vibroacoustics (Filippi *et al* [14]), it is  
95 applied here to structural dynamics with viscoelasticity. The method is a  
96 mathematically founded generalization of the classical modal approach to  
97 frequency dependent cases. Based on the use of the inverse Laplace trans-  
98 form, it requires a modeling technique combined to iterative or perturbation  
99 techniques. The finite element method has been selected for this purpose  
100 but the choice, however, is not restricted; the finite difference method or  
101 even analytical expressions could also be used. The example of an elas-

102 tomer with strong viscoelastic characteristics has been chosen to illustrate  
 103 the method.

## 104 2. Problem frequency formulation

### 105 2.1. Local equations

106 Assuming that the Laplace transform given by

$$\mathcal{L} \left[ \tilde{f}_i(t) \right] = f_i(s) = \int_0^\infty \tilde{f}_i(t) e^{-st} dt \quad (1)$$

107 is applied to the local constitutive equations of an isotropic viscoelastic  
 108 material, the following frequency representation is obtained:

$$\sigma_{ij}(s) = \frac{E'(s)(1+i \tan \delta(s))}{1+\nu} \left[ \epsilon_{ij}(s) + \frac{\nu}{1-2\nu} \epsilon_{kk}(s) \delta_{ij} \right], \quad (2)$$

109 where  $\sigma_{ij}$  is the stress tensor,  $\epsilon_{ij}$  the strain tensor,  $\nu$  Poisson's ratio and  $\delta_{ij}$   
 110 Kronecker symbol.  $E'(s)$  is the storage modulus, while  $\tan \delta(s)$  is associated  
 111 to the material energy loss. Both can be expressed as polynomial curve-  
 112 fittings of tabular experimental data, as displayed in Figures 1 and 2. In  
 113 these figures, a frequency stiffening typical of elastomers can be observed,  
 114 as well as a frequency region around 60000 Hz, around which damping is  
 115 particularly large. Poisson's ratio is set equal to a constant but it is not a  
 116 restriction. Anisotropic viscoelastic properties could also be handled by the  
 117 method.

118

119 The problem statement is completed by boundary conditions and the fol-  
 120 lowing local equation of motion:

$$s^2 \rho u_i(s) - \sigma_{ij,j}(s) = f_i(s) + s \rho u_{i0} + \rho \dot{u}_{i0} \quad (3)$$

121 where  $u_i(s)$  is the local displacement,  $\rho$  the material density,  $f_i(s)$  a volume  
 122 force,  $u_{i0}$  an initial displacement and  $\dot{u}_{i0}$  an initial velocity.

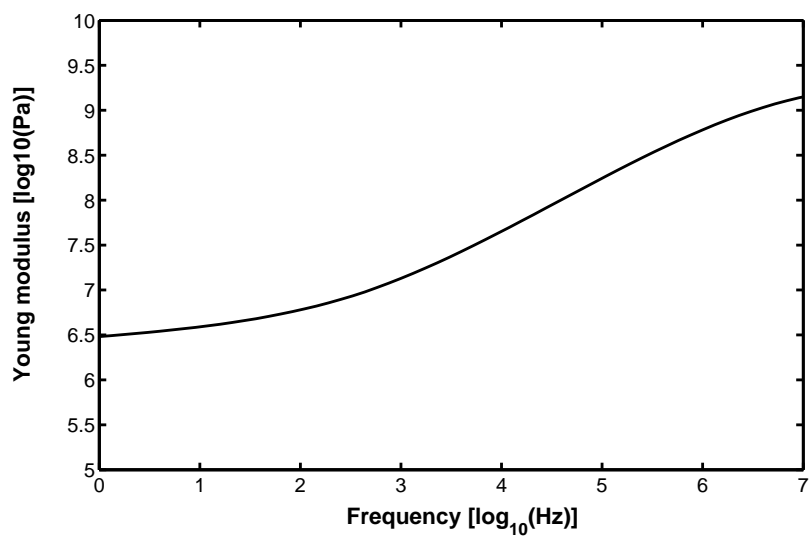


Figure 1: *Elastomer frequency-dependent storage modulus.*

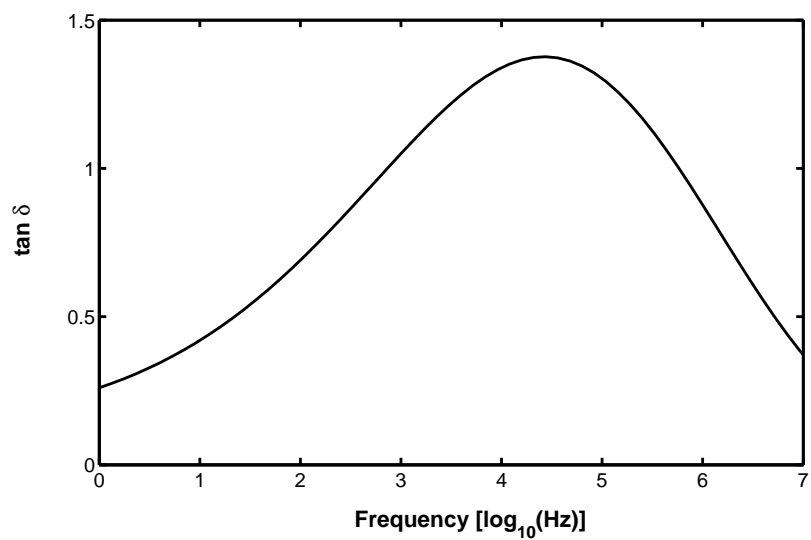


Figure 2: *Elastomer frequency-dependent tan δ.*

123 *2.2. Finite element formulation*

124 Local equations are multiplied by a conjugate weighting function and  
125 integrated over the structure volume (Ohayon and Soize [15]). Integrat-  
126 ing by part and using Bubnov-Galerkin method (Hughes [16]) with homo-  
127 geneous boundary conditions results in the following complex symmetric  
128 matrix problem:

$$[s^2M + K^B(s) + K^A] u(s) = F(s) + sI_0 + V_0 \quad (4)$$

129 where  $M$  is the mass matrix,  $u(s)$  the displacement solution vector,  $F(s)$   
130 the excitation force vector,  $I_0$  and  $V_0$  the initial displacement and velocity  
131 vectors, respectively. The stiffness matrix has been split into a frequency-  
132 independent part  $K^A$  and a frequency-dependent one  $K^B(s)$ . All matrices  
133 are generated by a 27-nodes fully quadratic solid element that gives a great  
134 flexibility for designing new damping treatments. A specific formulation  
135 with four pressure nodes per element has also been implemented to handle  
136 quasi-incompressibility. Bathe [17] emphasizes the good convergence qual-  
137 ities of this quasi-incompressible element. The main disadvantage of the  
138 current strategy is that it results in a bad conditioning of the matrix inver-  
139 sion problem that restricts the overall model size. As pointed out before,  
140 though, the resonance modes method is applicable to any kind of modeling  
141 technique.

142

143 The system is defined at a given value of the Laplace parameter  $s$  asso-  
144 ciated to a specific angular frequency  $\omega$  via  $s = \iota\omega$ , where  $\iota$  is the complex  
145 imaginary number. Classical solving methods such as the direct solution,  
146 which inverts the left-hand side operator of Equation (4), or the modal res-  
147 olution, which uses a biorthonormality relationship valid at fixed  $s$ , need  
148 both a discretization of the frequency axis. As many matrix factorizations  
149 as points on the frequency axis need to be computed, which, in the case of  
150 broadband excitations, results in very long solving times.

151 **3. Problem solution**

152 *3.1. The classical modal approach*

153 The modal resolution is based on the eigenvalue problem deduced from  
154 the homogeneous form of Equation (4):

$$[s_k^2(s) M + K^B(s) + K^A] u_k(s) = 0, \quad (5)$$

155 where  $(s_k(s), u_k(s))$  is the  $k^{th}$  eigenelement. This eigenvalue problem is  
156 complex, nonlinear in frequency and results in complex mode shapes. Since  
157 matrices are symmetrical by construction, following biorthonormality rela-  
158 tionship holds at fixed  $s$ :

$$\begin{cases} u_i^T(s) M u_j(s) = \delta_{ij} \\ u_i^T(s) [sK^B(s) + K^A] u_j(s) = -s_j^2(s) \delta_{ij} \end{cases} \quad (6)$$

159 Equation (4) solution  $u(s)$  is sought using the combination  $u(s) = \sum_i^N \alpha_i(s) u_i(s)$   
160 of the modes  $u_i(s)$  computed at  $s$ . Multiplying the equation with the trans-  
161 posed eigenvector  $u_j^T(s)$  yields:

$$u_j^T(s) [s^2 M + K^B(s) + K^A] \sum_i^N \alpha_i(s) u_i(s) = u_j^T(s) [F(s) + sI_0 + V_0]. \quad (7)$$

162 The frequency dependent coefficients  $\alpha_j(s)$  are easily determined using  
163 biorthonormality relationships (6). The displacement is finally given with  
164 respect to Laplace parameter  $s$  by

$$u(s) = \sum_i^N \frac{u_i^T(s) [F(s) + sI_0 + V_0]}{s^2 - s_i^2(s)} u_i(s) \quad (8)$$

165 It is worth pointing out that using relationship (8) is numerically ineffi-  
166 cient. In this case, a linearized form of Equation (5) with constant system  
167 matrices is obtained at each point of the frequency axis by setting  $s$ . The  
168 corresponding eigenvalue problem can be solved in a classical way, but its  
169 solution is valid at this specific frequency only. A considerable amount of

170 eigenvalue problems needs thus to be solved to compute the response over  
 171 a wide frequency band. It results in longer computation times than with  
 172 the direct solution.

### 173 3.2. Time solution

174 The time solution can be deduced from Equation (8) with Mellin-Fourier  
 175 inverse integral transform or Bromvitch formula expressed as following:

$$\mathcal{L}^{-1}[f(s)] = Y(t) f(t) = \frac{1}{2\pi i} \int_{C-i\infty}^{C+i\infty} f(s) e^{st} ds \quad (9)$$

176 where  $Y(t)$  is the Heaviside function,  $C$  the abscissa of the integration  
 177 vertical axis. Details of similar calculations made in the Fourier domain can  
 178 be found in the work by Filippi *et al* [14]. Let's focus on the computation  
 179 of the  $j^{th}$  term of Equation (8) sum only, associated to the dynamic loading  
 180  $F(s)$ , for clarity reasons. This term is given by:

$$U^j(s) = \frac{u_j^T(s) F(s) u_j(s)}{s^2 - s_j^2(s)} = \Psi(s) \frac{u_j^T(s) \phi u_j(s)}{s^2 - s_j^2(s)} \quad (10)$$

181 The excitation vector  $F(s)$  has been split into a frequency-dependent part  
 182  $\Psi(s)$  and a spatial one  $\phi$ . The inversion formula can thus be written as  
 183 following:

$$Y(t) u^j(t) = \frac{1}{2\pi i} \int_{C-i\infty}^{C+i\infty} \Psi(s) \frac{u_j^T(s) \phi u_j(s)}{s^2 - s_j^2(s)} e^{st} ds \quad (11)$$

184 If the denominator only consists of simple poles  $\hat{s}_j$ , the residue theorem  
 185 gives the time solution as the sum of following residues:

$$\begin{aligned} Res(\phi, \hat{s}_j) &= \lim_{s \rightarrow \hat{s}_j} \Psi(s) (s - s_j(s)) \frac{u_j^T(s) \phi u_j(s)}{s^2 - s_j^2(s)} e^{st} \\ &= \lim_{s \rightarrow \hat{s}_j} \Psi(s) \frac{u_j^T(s) \phi u_j(s)}{s + s_j(s)} e^{st} = \Psi(\hat{s}_j) \frac{u_j^T(\hat{s}_j) \phi u_j(\hat{s}_j)}{2\hat{s}_j} e^{\hat{s}_j t} \end{aligned} \quad (12)$$

186 Determining the  $j^{th}$  residue requires to find the  $j^{th}$  resonance pair  $(\hat{s}_j, \hat{u}_j)$   
 187 given by a limit calculation:

$$\begin{aligned} \lim_{s \rightarrow \hat{s}_j} [s_j^2(s) M + K^B(s) + K^A] u_j(s) \\ = [\hat{s}_j^2 M + K^B(\hat{s}_j) + K^A] \hat{u}_j = 0 \end{aligned} \quad (13)$$

188 This equation, called resonance value problem equation, is different from  
 189 the eigenvalue problem Equation (5). It is worth noting that resonance  
 190 pairs  $(\hat{s}_j, \hat{u}_j)$ , contrary to eigenpairs  $(s_j(s), u_j(s))$ , do not depend on fre-  
 191 quency. Resonance pairs are computed with a linear complex eigensolver  
 192 and a perturbation or an iterative scheme, which performs the limit calcu-  
 193 lation numerically.

194

195 Since the Laplace transform of a function  $f$  is such that  $f(\bar{s}) = \overline{f(s)}$ ,  
 196  $\bar{\hat{s}}_j$  is also solution of the resonance value problem (13). A second residue,  
 197 simply deduced from the first one by following relationship, needs thus to  
 198 be considered:

$$Res(\phi, \bar{\hat{s}}_j) = \overline{Res(\phi, \hat{s}_j)} \quad (14)$$

199 The part of the time response associated to the  $j^{th}$  term of the sum is finally  
 200 deduced by taking both residues into account:

$$Y(t) u^j(t) = \Re \left[ \Psi(\hat{s}_j) \frac{u_j^T(\hat{s}_j) \phi u_j(\hat{s}_j)}{\hat{s}_j} e^{\hat{s}_j t} \right] \quad (15)$$

201 where  $\Re(z)$  stands for the real part of the complex number  $z$ . The complete  
 202 time solution has following final form (for  $t \geq 0$ ):

$$u(t) = \sum_{j=1}^N \Re \left[ \frac{u_j^T(\hat{s}_j) \phi u_j(\hat{s}_j)}{\hat{s}_j} \psi(t) * e^{\hat{s}_j t} + u_j^T(\hat{s}_j) \left( I_0 + \frac{V_0}{\hat{s}_j} \right) u_j(\hat{s}_j) e^{\hat{s}_j t} \right] \quad (16)$$

203 where  $\psi(t)$  is the time representation of the excitation spectrum  $\Psi(s)$  and  
 204 the symbol  $*$  the convolution product. There are numerous advantages to  
 205 using this analytical expression. Once resonance modes have been com-  
 206 puted, Eq. (16) is easy to calculate and accurate. It is also valid for non-  
 207 stationary excitation types. Any new excitation case can be considered with  
 208 little additional computational cost compared to most transient methods.  
 209 The resonance modes method can thus be seen as a generalization of the  
 210 modal approach to the linear viscoelastic case. No hypothesis is made on  
 211 the damping type; this one can be specified by a simple curve fitting of tab-  
 212 ular data. The existence of the Laplace transform of an implicit viscoelastic

213 stiffness tensor defined in the time domain, which is however not needed in  
 214 the calculation, is the only hypothesis.

### 215 3.3. Frequency solution

216 The frequency response is finally obtained by computing the Laplace  
 217 transform of Equation (16). The displacement solution  $u(s)$  is given by  
 218 following relationship:

$$\begin{aligned}
 u(s) = \frac{1}{2} \sum_{j=1}^N & \left\{ \left[ u_j^T(\hat{s}_j) \frac{\phi \Psi(s) + \hat{s}_j I_0 + V_0}{\hat{s}_j (s - \hat{s}_j)} u_j(\hat{s}_j) \right] \right. \\
 & \left. + \left[ \bar{u}_j^T(\hat{s}_j) \frac{\phi \Psi(\bar{s}) + \bar{s}_j I_0 + V_0}{\bar{s}_j (s - \bar{s}_j)} \bar{u}_j(\hat{s}_j) \right] \right\} \quad (17)
 \end{aligned}$$

219 This expression has to be compared with the expression obtained with  
 220 the classical modal approach in the non-proportional damping case (Equa-  
 221 tion (8)). The classical modal approach requires one to compute an eigen-  
 222 value problem per frequency axis point, while the resonance modes method  
 223 requires one to solve a number of eigenvalue problems that depends on the  
 224 selected strategy to spot resonance modes.

## 225 4. The numerical computation of resonance modes

226 Resonance modes can be computed with a linear complex eigensolver  
 227 combined with search techniques that make repeated calls to the solver.  
 228 Search techniques are presented in the forthcoming paragraph. The imple-  
 229 mented complex eigensolver is then described in the following paragraph.

### 230 4.1. Looking for the resonance modes

231 Several approaches can be used to spot resonance modes. Three of them  
 232 have been implemented and compared. The first one, based on matrix  
 233 Equation (5), is iterative, and focuses on each resonance mode separately.  
 234 Araújo *et al* [18] used a similar technique to track the modes of sandwich  
 235 laminated plates with viscoelastic core in order to obtain enhanced damp-  
 236 ing estimations. The authors, however, did not go forward by making use

237 of the resonance modes to compute the response and an inefficient direct  
238 approach is used instead.

239

240 In the first step of the iterative approach, the viscoelastic matrix  $K^B(s_0)$  is  
241 constructed at a fixed parameter value  $s_0$  based on an estimation of the first  
242 resonance frequency. If no prior knowledge of this frequency is available,  
243 as it will be assumed later in the numerical examples, one can simply set  
244  $s_0$  to zero, but it may deteriorate the convergence slightly. Setting a value  
245 for  $s$  makes the complex eigenproblem linear and solvable. Once the eigen-  
246 solver has been called, the eigenvalue of the mode of interest that has just  
247 been computed is used to create an updated viscoelastic matrix  $K^B(s_1)$ .  
248 The process is then reiterated. After repeated calls to the eigensolver, the  
249 scheme converges toward a resonance mode as defined by Equation (13).  
250 The Arnoldi method, implemented in the eigensolver described in the next  
251 paragraph, remains efficient when many eigenvalues are extracted simulta-  
252 neously. This is why a few eigenvalues are actually computed to initialize  
253 the algorithm properly when the next resonance modes are sought.

254

255 The chosen convergence criterion is based on the frequency difference ratio  
256 between two successive iterations. Convergence is considered to be reached  
257 when the ratio is lower than  $10^{-3}\%$ . It has always been observed in all the  
258 numerical examples of the paper. Three iterations seem necessary to spot  
259 the first resonance mode, since the program may start with a poor estimate  
260 of the first resonance frequency, while two iterations are then required for  
261 each subsequent mode, since a better estimation is available. The algo-  
262 rithm, based on this iterative method, is given the identification label **A1**.  
263 It could further be improved by adding a mode shape identification routine  
264 to distinguish very closely spaced modes that might be mixed up during the  
265 iteration process. The structural examples that will be considered in the  
266 next paragraph, however, have not required this additional feature.

267

268 The second and third search approaches use a perturbation technique. This  
 269 technique is based on an algebra theorem (Lascaux and Théodor [19]), which  
 270 gives the analytical expression of new eigenvalues obtained when the stiff-  
 271 ness matrix is perturbed by a matrix  $C$  and a small parameter  $\epsilon$ . The theo-  
 272 rem is formulated as following: *Let  $\lambda_k$  be a simple eigenvalue of the diago-*  
 273 *nalizable matrix  $K$  and  $\lambda_k(\epsilon)$  the corresponding one associated to  $K + \epsilon C$ , so*  
 274 *that  $\lim_{\epsilon \rightarrow 0} \lambda_k(\epsilon) = \lambda_k$ . For a sufficiently small  $\epsilon$ , following results apply:*

$$275 \begin{cases} \lambda_k(\epsilon) = \lambda_k + \epsilon (v_k^H C u_k) + O(\epsilon^2) \\ u_k(\epsilon) = u_k + \epsilon \left( \sum_{i=1, i \neq k}^N \frac{v_i^H C u_k}{\lambda_k - \lambda_i} u_i \right) + O(\epsilon^2) \end{cases} \quad (18)$$

276 where  $v_k^H$  is the hermitian transpose of the  $k^{th}$  left eigenvector. The same  
 277 relationships hold for generalized eigenproblems after mass-matrix orthonor-  
 278 malization. As far as complex symmetric eigenproblems concerns, left eigen-  
 279 vectors are simply deduced from their right counterpart  $u_k$  using  $u_k = \bar{v}_k$ .  
 280 This theorem can be used to determine a better estimation of the next reso-  
 281 nance mode from a first eigenvalue computation. Let's assume for instance  
 282 that a first resonance mode of frequency  $f_1$  associated to Laplace param-  
 283 eter  $\hat{s}_1$  has been computed. The next resonance mode associated to Laplace  
 284 parameter  $\hat{s}_2$  is now targeted. An approximation  $s_2(f_1)$  is already available,  
 285 since the second eigenvalue of the system constructed at frequency  $f_1$  has  
 286 been extracted in a previous step. A perturbation matrix  $\Delta K$ , which takes  
 287 the frequency effect into account, is built as following:

$$\Delta K^B = K^B(s_2(f_1)) - K^B(\hat{s}_1) \quad (19)$$

288 An improved estimation of  $\hat{s}_2$  can then be deduced from the perturbation  
 289 technique:

$$\hat{s}_2^2 \approx s_2^2(f_1) + u_2^T(f_1) \Delta K^B u_2(f_1) \quad (20)$$

290 where  $u_2(f_1)$  is the second mode shape of the system constructed at fre-  
 291 quency  $f_1$ . This expression can be used to accelerate the iterative scheme.  
 292 It has been implemented in an algorithm combining perturbation and iter-  
 293 ation, identified by label **A2**. In practice, two iterations only are needed to

294 determine the first resonance mode, instead of three with a pure iterative  
 295 approach. Only one iteration instead of two is necessary for the next res-  
 296 onance modes. The algorithm **A2** thus needs to solve approximately one  
 297 eigenvalue problem per resonance mode, roughly half as many as in algo-  
 298 rithm **A1**.

299

300 It is also possible to use the perturbation method from the results of a  
 301 single eigenvalue problem computation. The middle of the frequency range  
 302 is taken as reference to build up the viscoelastic matrix  $K_V$ . In doing so,  
 303 it is assumed that minimizing the maximum coefficient of all perturbation  
 304 matrices will increase the validity domain of the local approximation. Fur-  
 305 ther investigations in the field of perturbation analysis should be carried  
 306 out to determine an optimal reference frequency. All modes are computed  
 307 instead of just a few. The eigenvalues are then adjusted successively. This  
 308 approach has been implemented in a fast algorithm identified by label **A3**.

#### 309 4.2. A complex eigensolver

310 A symmetric complex eigensolver has been implemented using ARPACK  
 311 library [20], based on the *Implicitly Restarted Arnoldi Method*. It can be  
 312 considered as an extrapolation of Lanczos method to general structured  
 313 matrices that have a certain degree of sparsity. ARPACK works by calling  
 314 user-supplied routines repeatedly via a reverse communication interface.  
 315 The user is thus free to choose any convenient data structure or matrix  
 316 inversion algorithm. Cholesky factorization could be used to reshape the  
 317 eigenvalue problem generalized form into a standard one, since the mass  
 318 matrix is symmetric positive-definite. However, the shift-invert mode for  
 319 generalized problems has been chosen. This mode is more efficient when  
 320 only a few localized eigenvalues are sought (algorithms **A1** and **A2**). If a  
 321 spectral shift  $\sigma$  is introduced in the eigenvalue problem, following equation  
 322 is obtained:

$$(K - \lambda M) u = (K - \sigma M - (\lambda - \sigma) M) u = 0 \quad (21)$$

323 where  $K$  is the stiffness matrix,  $M$  the mass matrix and  $(\lambda, u)$  an eigenpair.  
 324 The problem can be further transformed into the following one:

$$\left( \left( \frac{1}{\lambda - \sigma} \right) I - (K - \sigma M)^{-1} M \right) u = (\Lambda I - \tilde{K}) u = 0 \quad (22)$$

325 The matrix  $\tilde{K}$ , defined by

$$\tilde{K} = (K - \sigma M)^{-1} M \quad (23)$$

326 has been introduced. The Arnoldi method can compute the spectrum dom-  
 327 inant eigenpairs like  $(\Lambda, u)$  from the transformed system  $(\tilde{K}, I)$  efficiently.  
 328 The corresponding eigenvalue  $\lambda = \frac{1}{\Lambda} + \sigma$  of the initial matrix system  $(K,$   
 329  $M)$  can then be deduced. The convergence is quicker if  $\sigma$  is close to  $\lambda$ .  
 330 The system construction frequency thus gives an appropriate shift value  $\sigma$ ,  
 331 which is systematically updated during the iterative process and for each  
 332 new resonance mode.

333

334 An inversion algorithm needs to be provided in order to carry out cal-  
 335 culations such as  $y = \tilde{K}x$ , in which  $x$  is a vector given by ARPACK and  
 336  $y$  the vector requested by the reverse communication interface. Several  
 337 iterative methods using Krylov-subspaces such as the Restarted Gener-  
 338 alized Minimum Residual (RGMRES), the Conjugate Gradient Squared  
 339 (CGS), the Polynomial Stabilized bi-conjugate gradient (Bi-CGSTAB(l)),  
 340 or the TFQMR method (Transpose-Free Quasi-minimal Residual) have been  
 341 tested. These algorithms, available in the Numerical Algorithms Group li-  
 342 brary (NAG [21]), can be used in combination with three preconditioners  
 343 such as the Jacobi, SSOR (Symmetric Successive-Over-Relaxation), ILU  
 344 (incomplete LU factorization) preconditioners. The option without pre-  
 345 conditioning is also available. The only numerical drawback of the library  
 346 algorithms is their non-symmetric storage scheme that requires a memory  
 347 size doubling. Another solver computing the direct frontal solution has also  
 348 been implemented. The program uses routines from the SPARSEPAK li-  
 349 brary that have been modified to handle complex numbers. It also uses a

350 routine from the software METIS [22] that carries out graph partitioning  
351 and fill-reducing orderings of sparse matrices.

Aluminum Young's modulus	70 GPa
Aluminum Poisson ratio	0.3
Aluminum density	2700 kg.m <sup>-3</sup>
Aluminum damping	0
Elastomer density	1190 kg.m <sup>-3</sup>
Elastomer Poisson ratio	0.4875

Table 1: *Materials characteristics.*

352

353 Numerical tests have been conducted to compare the performances of the  
354 different eigensolvers. Complex symmetric matrices have been generated by  
355 modeling a 35 cm × 40 cm × 2 mm aluminum plate with free boundary  
356 conditions and a 10 cm × 10 cm damping patch located in a corner. All  
357 materials characteristics are summarized in Table 1. Aluminum damping  
358 is considered negligible here. The patch is made of a 1 mm-thick elastomer  
359 layer (characteristics displayed in Figures 1 and 2) constrained by a 0.5  
360 mm-thick aluminum layer. This type of damping treatment results in high  
361 levels of dissipation and is extensively used in the transportation industry.  
362 A unique eigenvalue problem constructed at 45 Hz, very close to the first  
363 structure non-rigid body mode, has been solved. This choice of frequency,  
364 although quite arbitrary, makes the inversion problem numerically hard to  
365 solve and seems well adapted to benchmark the algorithms. The whole  
366 procedure yields performance results in terms of CPU time and maximum  
367 memory usage that are useful to determine the best algorithmic option. It  
368 has been found, in particular, that only the ILU preconditioner makes the  
369 various iterative routines converge. It has also been found that all itera-  
370 tive routines behave in a similar way and give very close computation times  
371 and memory needs. Table 2 displays numerical comparisons between the  
372 two best solvers. The first one is the ILU/CGS iterative solver, while the  
373 second one computes the direct frontal solution. Each column of the table

374 represents a different system discretization and therefore a different matrix  
 375 size. The table clearly shows that the algorithm implementing the direct

Matrix size		387	891	1971	3051	4851
CPU time (s)	<b>ILU/CGS</b>	0.74	6.20	31.25	101.62	348.69
	<b>Direct</b>	0.15	0.42	1.14	2.32	4.16

Max. memory (MB)	<b>ILU/CGS</b>	0.98	0.98	59	91	150
	<b>Direct</b>	1	1	15	23	36

Table 2: Comparison between the ILU/CGS and the direct solution complex eigensolvers for various matrix sizes.

375  
 376 method is much more efficient than algorithms based on iterative methods.  
 377 The reason is related to the family type of interpolation functions used in  
 378 the finite element model. Quadratic elements yield populated matrices with  
 379 a bad conditioning for the iterative inversion problem.

## 380 5. Solvers comparison and validation

### 381 5.1. Response of a damped system

382 The response of a clamped plate to point-force excitation has been com-  
 383 puted using algorithms **A1**, **A2** and **A3**, which are different implemen-  
 384 tations of the resonance modes method. All three use the direct frontal  
 385 algorithm, the fill-reducing ordering algorithm as well as the shift-invert  
 386 strategy for generalized eigenvalue problems described in the previous para-  
 387 graph. **A1** uses the iterative technique presented in § 4.1, **A2** the hybrid  
 388 iterative/perturbation approach and **A3** the perturbation method. Two ad-  
 389 ditional algorithms that invert the left hand side operator of Equation (4)  
 390 have also been programmed and can be considered as reference implementa-  
 391 tions of current standards for frequency-dependent dynamic problems. The  
 392 first one, based on the direct frontal solution with fill-reducing ordering,  
 393 is called **Direct**, while the second one, which uses the classical modal ap-  
 394 proach (Equation (8)), is called **Eigenmodes**. A resolution of 1 Hz has

395 been chosen to discretize the frequency axis. This choice has a tremendous  
 396 impact on the computation time of these last two algorithms.

397

398 The modeled configuration is a 2mm-thick 35 cm  $\times$  40 cm clamped alu-  
 399 minum plate excited by a point force ( $x = 28$  cm,  $y = 20$  cm) of unit value  
 400 from 0 Hz to 1000 Hz. The displacement has been computed at a single  
 401 location ( $x = 28$  cm,  $y = 32$  cm). Two different treatment configurations  
 402 have been studied: a slightly damped configuration with a 6.9 cm  $\times$  8.9 cm  
 403 constrained elastomer patch located at the center of the plate and a very  
 404 damped configuration with a patch covering it. The patches are made of a 1  
 405 mm-thick elastomer layer (characteristics displayed in Figures 1 and 2) con-  
 406 strained by a 0.5 mm-thick aluminum layer. The materials characteristics  
 407 are given in Table 1, while Table 3 summarizes the numerical characteristics  
 408 of both configurations.

409

Case	Slightly damped	Very damped
Plate mesh	$20 \times 20$	$20 \times 20$
Number of elements	480	1600
Matrix size	$\sim 16000$	$\sim 44000$
Number of matrix coefficients	$\sim 2.2 \cdot 10^6$	$\sim 7.4 \cdot 10^6$

Table 3: *Numerical characteristics of the two studied plate configurations.*

410 A number of indicators are output to analyze the performances of all  
 411 five solvers. The CPU time has been estimated and normalized by dividing  
 412 it to the five solvers minimum value. Other characteristics such as the max-  
 413 imum memory required, the number of system resolutions or the number of  
 414 factorizations have also been measured.

415 5.2. *The slightly damped case*

416 The computation characteristics of all five algorithms are displayed in  
 417 Table 4 for the slightly damped case. It can be noticed that the number of  
 418 system constructions, factorizations and resolutions is equal to 999 in the  
 419 case of the direct solution. It corresponds to the number of points on the  
 420 frequency axis. A configuration with no frequency dependence would have  
 421 required a unique factorization and the same number of resolutions, result-  
 422 ing in a much smaller computation time, since factorizations are numerically  
 423 very intensive. The classical modal solution also needs a factorization per  
 424 frequency but a larger number of resolutions, which makes it even less appro-  
 425 priate than the direct solution to solve problems with frequency dependent  
 426 characteristics. Iterative versions of the resonance modes method, on the  
 427 other hand, require a number of factorizations related to the number of  
 428 modes located in the frequency band of interest (15 resonance modes in the  
 429 current case). Only the implementation with perturbation needs a unique  
 430 factorization. The observed CPU time, as shown in Table 4, are consistent  
 431 with these figures. The hybrid iterative/perturbation solver **A2** is roughly  
 432 20 times faster than the direct resolution, while the very fast perturbation  
 433 solver **A3** is about 200 times faster.

	<b>Resonance modes</b>				
	<b>Direct</b>	<b>Eigenmodes</b>	<b>A1</b>	<b>A2</b>	<b>A3</b>
Normalized CPU time	191	295	16	10	1
Max. memory (MB)	86	91	112	112	112
Factorizations number	999	999	31	16	1
Resolutions number	999	1921	1921	976	60

Table 4: *Direct solution, modal resolution and resonance-based **A1**, **A2** and **A3** algorithms performance comparison. Frequency response computation of the slightly damped plate configuration to point-force excitation.*

434

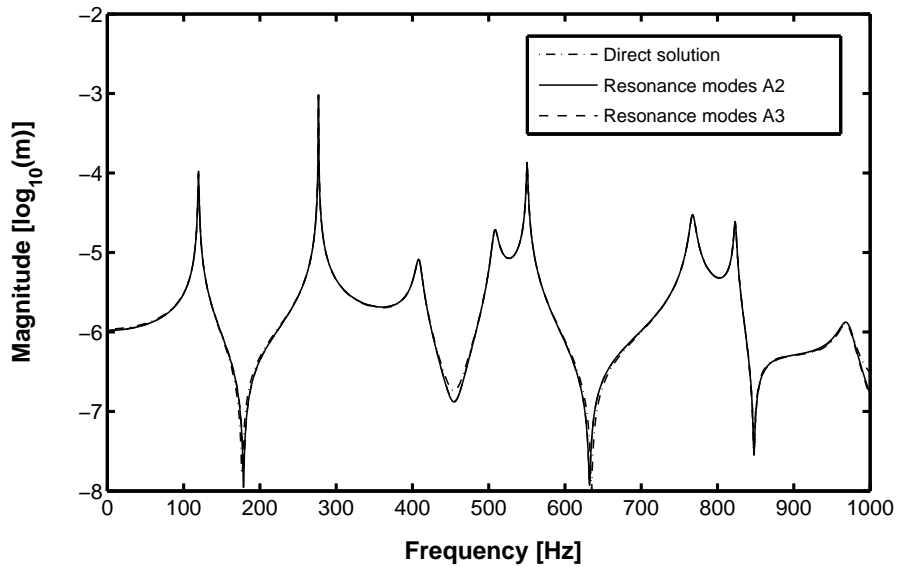


Figure 3: *Plate response to point force excitation in the slightly damped case*

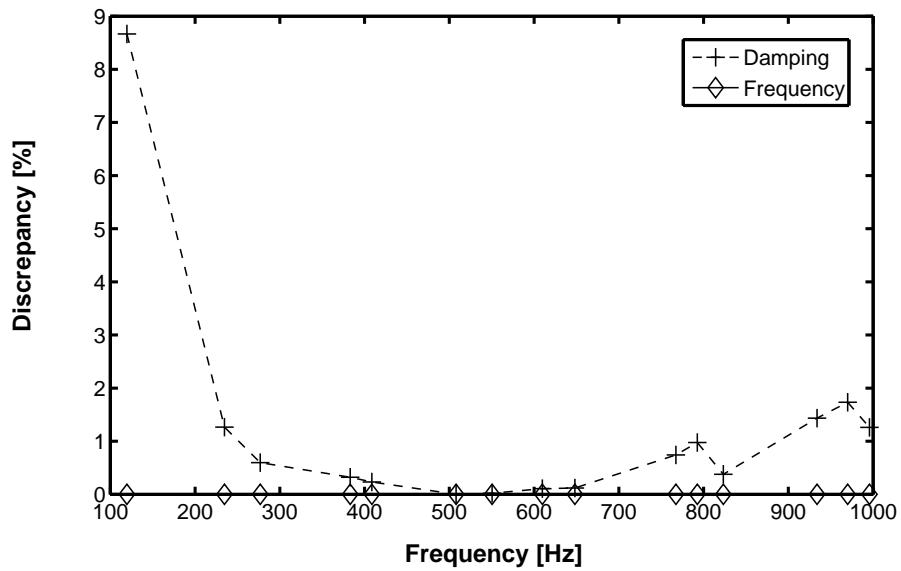


Figure 4: *Modal characteristics discrepancy between the perturbation algorithm **A3** and the iterative/perturbation one **A2**, with respect to the resonance modes frequency. Slightly damped case.*

435 The computed frequency response functions are displayed in Figure 3. Re-  
436 sults associated to the algorithm **Eigenmodes** based on the classical modal  
437 approach are not displayed, for clarity reasons. The direct resolution curve  
438 has been plotted instead, since it can be considered as being the reference  
439 in terms of accuracy. Algorithms **A1** and **A2** give identical results because  
440 the same convergence criterion is used for both routines; therefore only **A2**  
441 results are displayed. The figure shows a very good agreement between the  
442 resonance modes method and the direct resolution. Resonance modes algo-  
443 rithms **A2** and **A3** also show very similar results.

444  
445 Since algorithm **A3**, based on the perturbation method, yields approxi-  
446 mate modal quantities, it is worth comparing them with those computed  
447 by solver **A2**. The error on frequency and damping, expressed as a percent  
448 with respect to frequency, is displayed in Figure 4. The damping parameter  
449  $\alpha$ , expressed in Hz, is computed from the imaginary part of the complex  
450 resonance angular frequency  $\Omega = \omega + i\alpha$ , where  $\omega$  is the real angular fre-  
451 quency in  $\text{rad.s}^{-1}$ . Classical measures of damping, such as the loss factor  
452  $\eta$  or the inverse of the quality factor  $Q^{-1}$  can easily be deduced using the  
453 formula  $\eta = Q^{-1} = \alpha / \pi f$ , where  $f$  is the frequency in Hz. The error  
454 on the resonance modes frequencies is found negligible for all modes. As  
455 far as damping concerns, a maximum error of 9% is observed for the very  
456 first mode, but it is less than 1% on the major part of the spectrum. The  
457 minimum error is found at 500 Hz where the reference system has been  
458 constructed. The error on damping has a direct impact on the maxima of  
459 the frequency response function, but it is barely noticeable when using a  
460 logarithmic scale like in Figure 3.

### 461 5.3. *The very damped case*

462 The numerical characteristics associated to the five algorithms are dis-  
463 played in Table 5 for the configuration of a constrained elastomer patch  
464 covering the plate entirely. Apart from the patch size, all other model char-  
465 acteristics (plate dimensions, materials, excitation and measurement point

466 location) remain unchanged.

	Resonance modes				
	Direct	Eigenmodes	A1	A2	A3
Normalized CPU time	404	486	32	21	1
Max. memory (MB)	413	425	454	455	457
Factorizations number	999	999	51	31	1
Resolutions number	999	26095	3289	1938	63

Table 5: *Direct solution, modal resolution and resonance-based A1, A2 and A3 algorithms performance comparison. Frequency response computation of the very damped plate configuration to point-force excitation.*

467

468 There are two main differences with previous computation. First, the sys-  
469 tem is heavily damped due to the large patch. Second, roughly three times  
470 more elements are needed to model the three layers sandwich (see Table 3).  
471 The eigenvalue problem is thus harder to solve, as one can notice by com-  
472 paring the number of resolutions required by the algorithms **Eigenmodes**  
473 and **Direct**. Twice as many resonance modes as before (30 in total) are  
474 used to compute the response on the frequency band of interest. The 17<sup>th</sup>  
475 resonance mode is located around 1000 Hz while the 30<sup>th</sup> is very close to  
476 1600 Hz. The solver **A2** remains however very efficient compared to the  
477 direct solution with CPU times that are about 20 times smaller. Solver  
478 **A3** is roughly 400 times faster than the direct solution solver. The fre-  
479 quency response functions obtained with algorithms **A2**, **A3** and **Direct**  
480 are displayed in Figure 5. A 30 modes-basis has been selected for the first  
481 two algorithms and is compared with a 60 modes-basis. Results given by  
482 the resonance modes method are very similar and compare also well with  
483 the direct solution results. Maxima are consistently estimated by all three  
484 algorithms. A slight discrepancy between the curves can be observed at the  
485 responses minima, in particular around 0 Hz and 860 Hz. This is related

486 to the modal basis truncation, which alters the accuracy of the resonance  
 487 modes method just as it is observed with the classical modal method. It  
 488 is particularly detrimental to heavily damped structures, for which modes  
 489 contribution to the overall response is prevailing below their resonance. One  
 490 can notice that taking a larger modal basis constituted of 60 modes instead  
 491 of 30 results in enhanced results.

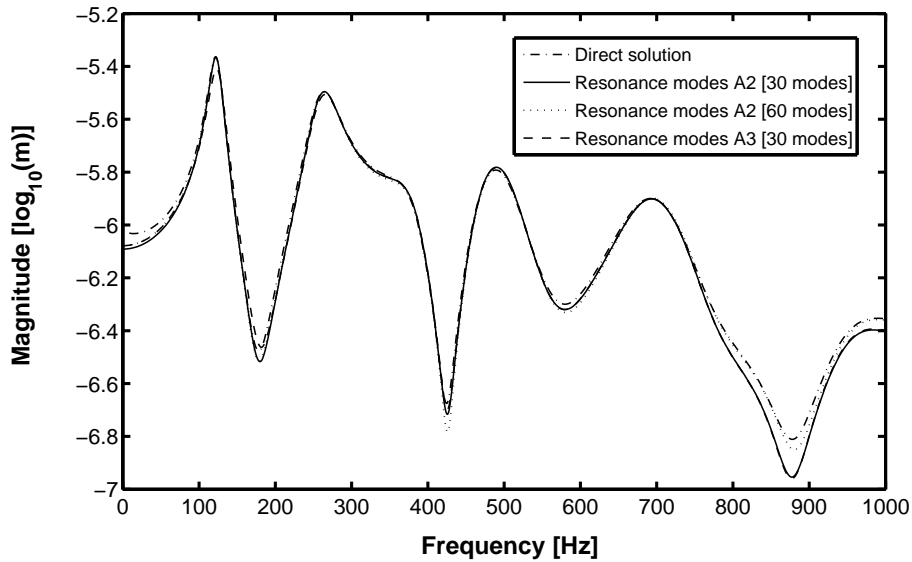


Figure 5: *Plate response to point force excitation in the very damped case*

492

493 The error ratio on resonance modes frequency and damping between solvers  
 494 **A2** and **A3** is displayed in Figure 6. The overall damping error ratio is small  
 495 in the upper frequency range, close to zero at the construction frequency  
 496 500 Hz, but increases as frequency reduces. A maximum error of 16% is  
 497 reached for the very first mode around 115 Hz. A possible refinement of al-  
 498 gorithm **A3** could be to include an additional construction point in the lower  
 499 frequency range, for instance around 150 Hz. The selection of additional  
 500 points should be adapted to the material frequency dependence displayed  
 501 in Figures 1 and 2. The figures show that both storage modulus and  $\tan \delta$

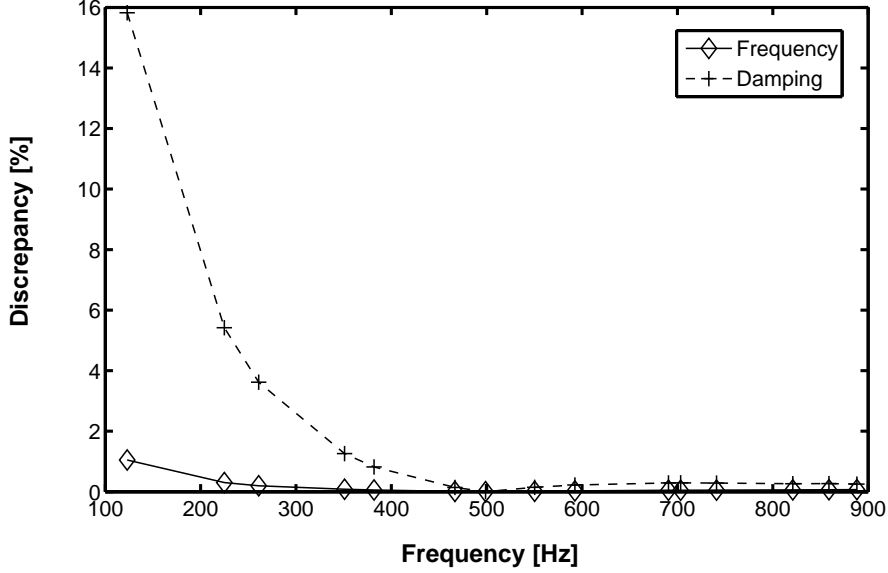


Figure 6: Modal characteristics discrepancy between the perturbation algorithm **A3** and the iterative/perturbation one **A2**, with respect to the resonance modes frequency. Very damped case.

502 have a linear behavior between 300 Hz and 1000 Hz. This is why solver  
 503 **A3** is very accurate for both the slightly and very damped cases within this  
 504 frequency band.

## 505 6. Vibroacoustic validation of the perturbation-based solver

### 506 6.1. The vibroacoustic system

507 A vibroacoustic validation of the fast perturbation-based solver **A3** is  
 508 presented now. The impact of the modal discrepancy between **A2** and  
 509 **A3** on the predicted noise, indeed, is worth being estimated since damping  
 510 treatments are often used to reduce noise. The acoustic power of the previ-  
 511 ous clamped plate configurations with two different patch sizes is computed  
 512 by assuming baffled conditions of radiation. In the vibroacoustic case, the  
 513 matrix system (4) associated to the structure can be written in an energy

514 form as follows:

$$w^T(s) [s^2 M + K^B(s) + K^A] u(s) - P(w(s), u(s), s) = w(s)^T (F(s) + sI_0 + V_0) \quad (24)$$

515 where  $w(s)$  is a displacement,  $P(w, u, s)$  a vibroacoustic coupling operator  
 516 that takes normal stress continuity at the solid/fluid interface into account.  
 517 In the case of a flat plate perpendicular to the vertical direction, it can be  
 518 written as a combination of the pressure  $p(M, s)$  and the normal displace-  
 519 ment  $w(M, s)$  on the top face  $S_+$  and bottom face  $S_-$ :

$$P(w, p, s) = \int_{S_+} w(M, s) p(M, s) d_{S_M} - \int_{S_-} w(M, s) p(M, s) d_{S_M} \quad (25)$$

520 Assuming baffled conditions of radiation, the acoustic pressure can be mod-  
 521 eled using Rayleigh integral (Fahy [23]). On the top face, for instance,  
 522 the pressure is expressed with respect to the normal velocity  $u(M_0, s)$  as  
 523 following:

$$p(M, s) = \rho s^2 \int_{S_+} G(M_0, M, s) u(M_0, s) d_{S_{M_0}} \quad (26)$$

524 where  $G(M_0, M, s) = -\frac{e^{ikMM_0}}{4\pi MM_0} - \frac{e^{ikMM_1}}{4\pi MM_1}$  is the Green kernel for the Neumann  
 525 problem of the Helmholtz equation in a semi-infinite medium limited by the  
 526 plane occupied by the baffled structure,  $M_1$  is the image of  $M_0$  with respect  
 527 to this plane; for a problem in which the only source is the radiating baffled  
 528 structure,  $M_1$  coincide with  $M_0$  and one has  $G(M_0, M, s) = -\frac{e^{ikMM_0}}{2\pi MM_0}$ .  $k$  is  
 529 the wave number. On the bottom face, a negative sign, due to the negative  
 530 orientation of the face, is added. The acoustic coupling operator is finally  
 531 given by:

$$P(w, u, s) = \rho_f s^2 \left( \int_{S_+} \int_{S_+} w(M, s) G(M_0, M, s) u(M_0, s) d_{S_M} d_{S_{M_0}} \right. \\ \left. + \int_{S_-} \int_{S_-} w(M, s) G(M_0, M, s) u(M_0, s) d_{S_M} d_{S_{M_0}} \right) \quad (27)$$

532 This formulation takes the normal displacement of both faces into account  
 533 and is well adapted to a solid elements model able to assess strain along

534 the thickness. Numerically, the operator is evaluated by expressing the nor-  
535 mal displacement from the finite element degrees of freedom and quadratic  
536 functions to interpolate the values. When  $M_0$  and  $M$  belong to the same  
537 element, the Green function can become singular. A regularization of the  
538 singularity is carried out over the element face by writing the displacement  
539 in a local cylindrical coordinates system (de Lautour [24]). The Jacobian  
540 of the transformation regularizes the final expression. After regularization,  
541 a Gauss-Legendre integration scheme is used.

542

543 The vibroacoustic coupling has an impact on resonance modes: it creates  
544 a mass effect, lowering modal frequencies. It also causes structural dissipa-  
545 tion since vibration energy is extracted by acoustic radiation. These effects  
546 are evaluated by solving the coupled vibroacoustic problem. The selected  
547 method, which implements a perturbation technique, is presented in detail  
548 in Appendix A.1. It makes repeated calls to a subroutine that evaluates the  
549 coupling operator as described above. Once the vibroacoustic resonance  
550 problem has been solved, the structural response can be evaluated in the  
551 frequency domain using Equation (17) or in the time domain using Equa-  
552 tion (16).

553

554 The acoustic power  $\mathcal{P}_{ac}$  is computed by assuming steady state conditions,  
555 for which the following time/frequency equivalence applies

$$\begin{aligned} \mathcal{P}_{ac} &= \frac{1}{T} \int_0^T \int_S p(t, M) v(t, M) dM dt \\ &= \int_0^\infty \int_S \frac{1}{2} \Re [p(\omega, M) \bar{v}(\omega, M)] dM d\omega \end{aligned} \quad (28)$$

556 where  $\omega$  is the angular frequency associated to  $s$  by  $s = \iota\omega$ ,  $p(t, M)$  and  
557  $v(t, M)$  are the acoustic pressure and velocity at point  $M$  in the time do-  
558 main;  $p(\omega, M)$  and  $v(\omega, M)$  are their counterparts in the frequency domain.  
559 The conjugate velocity at point  $M$   $\bar{v}(\omega, M) = -\iota\omega u(\omega, M)$  is deduced from  
560 the displacement  $u(\omega, M)$  given by expression (17) with the resonance so-  
561 lutions of the complete vibroacoustic system.

562

563 Acoustic power spectral density levels can be deduced from the routine  
 564 computing the acoustic coupling operator given by Equation (27) using fol-  
 565 lowing expression:

$$L_{P_{ac}} = 10 \log_{10} \frac{\frac{1}{2} \operatorname{Re}[-s P(u, u, s)]}{\mathcal{P}_{ac}^{ref}} \quad (29)$$

566 where  $\mathcal{P}_{ac}^{ref} = 10^{-12} W$  (Pierce [25]).

## 567 6.2. Numerical comparison of the solvers

568 Acoustic power computations carried out with the reference hybrid it-  
 569 erative/perturbation solver **A2** and the perturbation-based solver **A3** are  
 570 shown in Figure 7 for the slightly damped case and in Figure 8 for the very  
 571 damped case. The construction frequency used by **A3** remains 500 Hz as in  
 572 the previous examples. Solvers **A2** and **A3** perform so similarly for either  
 573 case that it is hard to distinguish any difference between the curves. It can  
 574 thus be concluded that the very fast variant **A3** is not only validated for  
 575 dynamic but also for vibroacoustic cases.

## 576 7. Conclusions

577 A method for computing the non-stationary time and frequency response  
 578 of viscoelastic structures, called the resonance modes method, has been  
 579 presented. Based on the computation of the inverse Laplace transform,  
 580 it requires a modeling technique such as the Finite Element Method, a  
 581 complex solver able to solve linear complex eigenvalue problems and itera-  
 582 tive/perturbation routines in order to spot the resonance modes, which are  
 583 the free solutions of the system. The method, that can be seen as an ex-  
 584 trapolation of the classical modal approach to complex frequency-dependent  
 585 cases, is able to handle dissipative anisotropic materials characteristics ex-  
 586 pressed in raw data form. The case of an aluminum plate covered by either  
 587 a small or a large constrained elastomer patch has been used to benchmark  
 588 various methods: the classical modal method, the direct solution method,

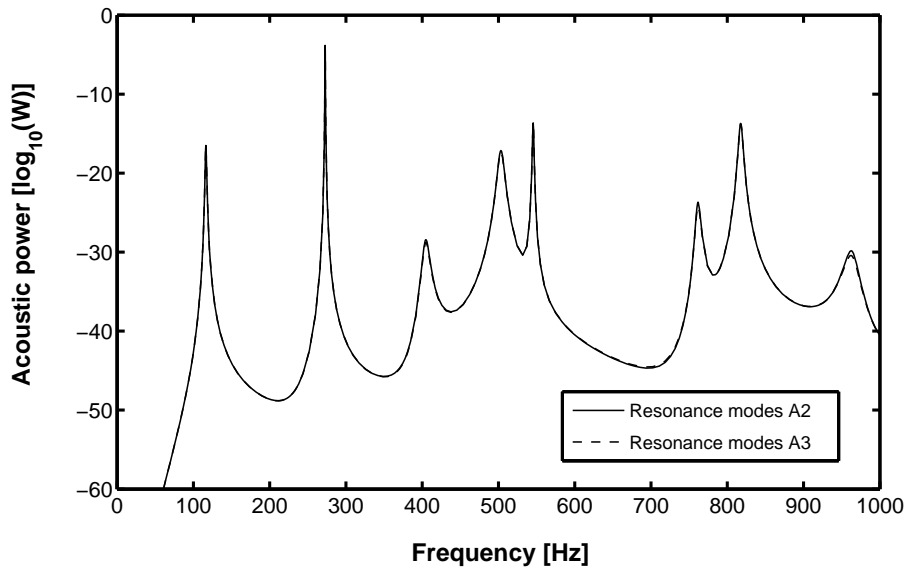


Figure 7: Comparison of the level of acoustic power using the iterative algorithm **A1** (reference) and the perturbation-based algorithm **A3**. Slightly damped case.

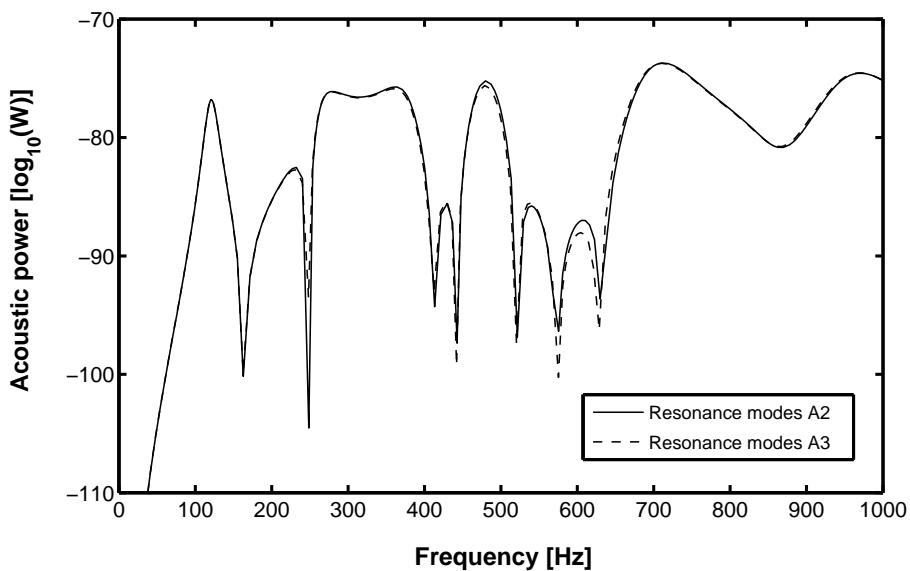


Figure 8: Comparison of the level of acoustic power using the iterative algorithm **A1** (reference) and the perturbation-based algorithm **A3**. Very damped case.

589 considered as the reference one, and three implementations of the resonance  
590 modes method. The first implementation uses an iterative approach to look  
591 for the resonance modes, while the second one, also iterative, is being accel-  
592 erated by perturbation. The third implementation is based on perturbation  
593 exclusively. The benchmark has shown that the resonance modes method  
594 results in much quicker computation times than the direct solution while  
595 keeping the same level of accuracy. The very quick variant, which provides  
596 computational times reduced by a factor of two in magnitude, has also been  
597 validated for vibroacoustic applications.

- 598 [1] J.-D. Chazot, B. Nennig, A. Chettah, Harmonic response computation of viscoelastic  
599 multilayered structures using a ZPST shell element, *Computers and Structures*, 89  
600 (2011) 2522-2530.
- 601 [2] I.C. Finegan, R.F. Gibson, Analytical modeling of damping at micromechanical  
602 level in polymer composites reinforced with coated fibers, *Composites science and  
603 technology* 60 (2000) 1077-1084.
- 604 [3] J. Woodhouse, Linear damping models for structural vibration, *Journal of sound  
605 and vibration* 215 (3) (1998) 547-569.
- 606 [4] P. Cha, Approximate eigensolutions for arbitrarily damped nearly proportional sys-  
607 tems, *Journal of sound and vibration* 288 (2005) 813-827.
- 608 [5] W.C. Hurty, M.F. Rubinstein, *Dynamics of structures*, Prentice-hall, 1964.
- 609 [6] S. Adhikari, An iterative approach for non proportionally damped systems, *Mechan-  
610 ics Research Communications* 38 (2011) 226-230.
- 611 [7] F. Cortés, M.J. Elejabarrieta, An approximate numerical method for the complex  
612 eigenproblem in systems characterised by a structural damping matrix, *Journal of  
613 Sound and Vibration*, 296 (2006) 166-182
- 614 [8] D.F. Golla, P.C. Hughes, Dynamics of viscoelastic structures - a time domain finite  
615 element formulation, *Journal of applied mechanics* 52 (1985) 897-906.
- 616 [9] F.S. Barbosa, M.C.R. Farage, A finite element model for sandwich viscoelastic  
617 beams: Experimental and numerical assessment, *Journal of sound and vibration*  
618 317 (2008) 91-111.
- 619 [10] G.A. Lesieutre, E. Bianchini, Time domain modeling of linear viscoelasticity using  
620 augmenting thermodynamic fields, *Journal of vibration and acoustics* 117 (1995)  
621 424-430.
- 622 [11] F. Cortés, M.J. Elejabarrieta, Forced response of a viscoelastically damped rod using  
623 the superposition of modal contribution functions, *Journal of Sound and Vibration*,  
624 315 (2008) 58-64
- 625 [12] S. Sorrentino, A. Fasana, Finite element analysis of vibrating linear systems with  
626 fractional derivative viscoelastic models, *Journal of Sound and Vibration*, 299 (2007)  
627 839-853
- 628 [13] C.-W. Kim, Damped dynamic response determination in the frequency domain for  
629 partially damped large scale structures, *Journal of Sound and Vibration*, 326 (2009)  
630 703-708

- 631 [14] P.J.T. Filippi, D. Habault, P-O. Mattei, C. Maury, The role of the resonance modes  
632 in the response of a fluid-loaded structure, *Journal of sound and vibration* 239 (4)  
633 (2001) 639-663.
- 634 [15] R. Ohayon, C. Soize, *Structural acoustics and vibration*, Academic Press, 1998.
- 635 [16] T.J.R. Hughes, *The finite element method*, Prentice-Hall, 1987.
- 636 [17] K.J. Bathe, *Finite element procedures*, Prentice-Hall, 1996.
- 637 [18] A.L. Araújo, C.M. Mota Soares, C.A. Mota Soares, J. Herskovits, Optimal design  
638 and parameter estimation of frequency dependent viscoelastic laminated sandwich  
639 composite plates, *Composite Structures* 92 (2010) 2321-2327.
- 640 [19] P. Lascaux, R. Théodor, *Analyse numérique matricielle appliquée à l'art de*  
641 *l'ingénieur, Méthodes directes*, Dunod, 2000.
- 642 [20] ARPACK, <http://www.caam.rice.edu/software/ARPACK>, 2013
- 643 [21] Numerical Algorithms Group (NAG), <http://www.nag.co.uk>, 2013
- 644 [22] METIS, <http://glaros.dtc.umn.edu/gkhome/views/metis>, 2013
- 645 [23] F. Fahy, Sound and structural vibration, *Academic press*, 1987.
- 646 [24] Nathaniel J. de Lautour, A galerkin method for the numerical analysis of diffraction  
647 by a rectangular screen, *Journal of the Acoustical Society of America* 106(6), 1999.
- 648 [25] Allan D. Pierce, *Acoustics. An Introduction to its Physical Principles and Applica-*  
649 *tions*, Acoustical Society of America, 1989.

## 650 **Appendix A. COMPUTATION OF THE VIBROACOUSTIC RES-** 651 **ONANCE MODES**

### 652 *Appendix A.1. Computation of the resonance values*

653 A perturbation technique has been used to compute the resonance modes  
654 of the damped vibroacoustic system. A weighting parameter  $\epsilon$  is introduced,  
655 the value of which varies from  $\epsilon = 0$  in the uncoupled case to  $\epsilon = 1$  in  
656 the fully coupled case. The resonance values problem can be expressed as  
657 following:

$$w^T [s_k(\epsilon)^2 M + K^B(s_k(\epsilon)) + K^A] u_k(\epsilon) = \epsilon P(w, u_k(\epsilon), s_k(\epsilon)) \quad (\text{A.1})$$

658 The zero-order matrix equation is obtained by setting  $\epsilon$  equal to zero:

$$[s_k(0)^2 M + K^B(s_k(0)) + K^A] u_k(0) = 0, \quad (\text{A.2})$$

659 where  $(s_k(0), u_k(0))$  is the  $k^{th}$  resonance couple of the damped system in  
 660 vacuum. The first derivative of (A.1) with respect to  $\epsilon$  is

$$\begin{aligned} & w^T \left[ s_k(\epsilon)^2 M + K^B(s_k(\epsilon)) + K^A \right] \frac{\partial}{\partial \epsilon} (u_k(\epsilon)) \\ & + w^T \left[ \frac{\partial}{\partial \epsilon} (s_k(\epsilon)^2) M + \frac{\partial}{\partial \epsilon} (K^B(s_k(\epsilon))) \right] u_k(\epsilon) \quad (\text{A.3}) \\ & = P(w, u_k(\epsilon), s_k(\epsilon)) + \epsilon \frac{\partial}{\partial \epsilon} (P(w, u_k(\epsilon), s_k(\epsilon))) \end{aligned}$$

661 The first-order matrix equation is obtained by letting  $\epsilon$  tend to zero and  
 662 taking Equation (A.2) into account:

$$w^T \left[ 2 \frac{\partial s_k(0)}{\partial \epsilon} s_k(0) M + \frac{\partial s_k(0)}{\partial \epsilon} \frac{\partial}{\partial s_k(0)} (K^B(s_k(0))) \right] u_k(0) = P(w, u_k(0), s_k(0)) \quad (\text{A.4})$$

663 Choosing  $w = \bar{u}_k(0)$  and orthonormalizing resonance vectors with the mass  
 664 matrix yields

$$\frac{\partial s_k(0)}{\partial \epsilon} = P(\bar{u}_k(0), u_k(0), s_k(0)) / \left[ 2s_k(0) + u_k(0)^H \left( \frac{\partial}{\partial s_k(0)} K^B(s_k(0)) \right) u_k(0) \right] \quad (\text{A.5})$$

665 The first-order approximation of the perturbed Laplace parameter is given  
 666 by  $s_k(\epsilon) = s_k(0) + \epsilon \frac{\partial s_k(0)}{\partial \epsilon}$ . When  $\epsilon = 1$ ,

$$\begin{aligned} s_k(1) & = s_k(0) + P(\bar{u}_k(0), u_k(0), s_k(0)) \\ & / \left[ 2s_k(0) + u_k(0)^H \frac{\partial}{\partial s_k(0)} (s_k(0) K^B(s_k(0))) u_k(0) \right] \quad (\text{A.6}) \end{aligned}$$

667 *Computation of the resonance vectors*

668 Similar developments can be written to assess the influence of the acous-  
 669 tic coupling on resonance vectors. Using Equation (A.3) and setting  $\epsilon$  equal  
 670 to zero yields

$$\begin{aligned} & w^T \left[ s_k(0)^2 M + K^B(s_k(0)) + K^A \right] \frac{\partial}{\partial \epsilon} (u_k(0)) \\ & = P(w, u_k(0), s_k(0)) - w^T \left[ \frac{\partial}{\partial \epsilon} (s_k(0)^2) M + \frac{\partial}{\partial \epsilon} (K^B(s_k(0))) \right] u_k(0) \quad (\text{A.7}) \end{aligned}$$

671 The equation left side operator spans a  $N-1$  dimensions space to which  
 672 vector  $u_k(0)$  does not belong. A decomposition on this operator basis can  
 673 be written as

$$\frac{\partial}{\partial \epsilon} (u_k(0)) = \sum_{i=1, i \neq k}^N \alpha_i u_i(0), \quad (\text{A.8})$$

674 Equation (A.7) can thus be further transformed into the following one

$$\begin{aligned} & w^T [s_k(0)^2 M + K^B(s_k(0)) + K^A] \frac{\partial}{\partial \epsilon} (u_k(0)) \\ &= w^T \sum_{i=1, i \neq k}^N \alpha_i [(s_k(0)^2 - s_i(0)^2) M + K^B(s_k(0)) - K^B(s_i(0))] u_i(0) \end{aligned} \quad (\text{A.9})$$

675 Coefficients  $\alpha_i$  are deduced by selecting  $w = \bar{u}_i(0)$  and by using the biorthonor-  
 676 mality properties of the symmetric system:

$$\begin{aligned} \alpha_i &= P(\bar{u}_i(0), u_k(0), s_k(0)) \\ &/ (s_k(0)^2 - s_i(0)^2 + u_i^H(0) [K^B(s_k(0)) - K^B(s_i(0))] u_i(0)) \end{aligned} \quad (\text{A.10})$$

677 The first order approximation of the  $k^{th}$  resonance vector of the damped  
 678 vibroacoustic structure is given by setting  $\epsilon = 1$ ,

$$u_k(1) = u_k(0) + \sum_{i=1, i \neq k}^N \alpha_i u_i(0) \quad (\text{A.11})$$

679 The intermodal coupling terms of this series have been found negligible  
 680 when the aluminum plate studied in this paper radiates in the air.